A&A 594, A60 (2016)
DOI: 10.1051/0004-6361/201628775

Astronomy & Astrophysics

VLBA observations of radio faint *Fermi*-LAT sources above 10 GeV

R. Lico[1], M. Giroletti[1], M. Orienti[1], and F. D'Ammando[1,2]

[1] INAF Istituto di Radioastronomia, via Gobetti 101, 40129 Bologna, Italy
e-mail: rocco.lico@unibo.it
[2] Dipartimento di Fisica e Astronomia, Università di Bologna, via Ranzani 1, 40127 Bologna, Italy

Received 22 April 2016 / Accepted 11 July 2016

ABSTRACT

Context. The first *Fermi*-LAT high-energy source catalog (1FHL), containing γ-ray sources detected above 10 GeV, is an ideal sample for characterizing the physical properties of the most extreme γ-ray sources.
Aims. We investigate the pc scale properties of a subsample of radio faint 1FHL sources with the aim of confirming the proposed blazar associations by revealing a compact high brightness temperature radio core, and we propose new low-frequency counterparts for the unassociated γ-ray sources (UGS). Moreover, we increase the number of 1FHL sources with high-resolution observations to explore the possible connection between radio and γ rays at $E > 10$ GeV.
Methods. We observed 84 1FHL sources, mostly blazars of high synchrotron peaked (HSP) type, in the northern sky with the Very Long Baseline Array (VLBA) at 5 GHz. These sources lack high-resolution radio observations and have at least one NRAO VLA sky survey counterpart within the 95% confidence radius. For those sources without a well-identified radio counterpart we exploit the VLBA multiple phase-center correlation capability to identify the possible low-frequency candidates.
Results. For ~93% of the sources in our sample we reveal a compact high brightness temperature radio core, which supports their proposed blazar association. The vast majority of the detected sources are radio weak, with a median VLBI flux density value of 16.3 mJy. For the detected sources we obtain an average brightness temperature on the order of 2×10^{10} K. We find a compact component for 16 UGS, for which we propose a new low-frequency association.
Conclusions. We find brightness temperature values that do not require high Doppler factors, and are in agreement with the expected values for the equipartition of energy between particles and magnetic field. We find strong indications for the blazar nature of all of the detected UGS, for which we propose new low-frequency associations. The characterization of the physical properties of this emerging population is relevant in view of the construction of the new generation Cherenkov Telescope Array.

Key words. galaxies: active – gamma rays: galaxies – BL Lacertae objects: general

1. Introduction

The vast majority of high-energy (HE, 100 MeV < E < 100 GeV) and very high-energy (VHE, $E > 0.1$ TeV) γ-ray sources are associated with radio loud objects, typically blazars, i.e., flat spectrum radio quasars (FSRQs) or BL Lac type objects (BL Lacs; e.g., Acero et al. 2015; Ackermann et al. 2015). Depending on the position of the peak of the synchrotron component of their spectral energy distribution (SED), blazars are further classified as low-, intermediate-, or high-synchrotron peaked (LSP, ISP, HSP) sources, characterized by a synchrotron peak frequency $\nu_{\rm peak}$ (Hz) such that $\log \nu_{\rm peak} < 14$, $14 < \log \nu_{\rm peak} < 15$, and $\log \nu_{\rm peak} > 15$, respectively (Abdo et al. 2010a).

In the MeV/GeV domain, the Large Area Telescope (LAT) on board the *Fermi* Gamma-ray telescope (*Fermi*) has provided a deep, uniform sky survey detecting as many as 3,033 sources in the *Fermi* third source catalog (3FGL, Acero et al. 2015). The results from *Fermi* show that both types of blazars are common HE emitters, with FSRQs having softer spectra and being generally more luminous than BL Lacs. Moreover, *Fermi* clearly revealed the existence of a highly significant correlation between the radio flux density and the γ-ray energy flux (Ackermann et al. 2011). However, observations from Imaging Atmospheric Cherenkov Telescopes (IACTs) preferentially detect BL Lac sources, in particular of the HSP type, and no evidence of a correlation between radio and VHE emission has been reported so far. The different demographics of the VHE population is explained by two main factors: FSRQs have softer spectra and are more distant, which decreases their VHE emission owing to extragalactic background light (EBL) absorption. The lack of a VHE-radio correlation may be due to the IACTs operational mode. The IACTs operate in pointing mode with a limited sky coverage, and they preferentially observe sources in a peculiar state. All of these limitations introduce a strong bias in VHE catalogs, and it is difficult to assess any possible radio-VHE correlation. Nonetheless, it is likely that some physical effect may also be at work.

The first *Fermi*-LAT catalog of sources above 10 GeV (1FHL, Ackermann et al. 2013) is an ideal resource for addressing the connection between HE and VHE emission. The 1FHL is based on LAT data accumulated during the first three years of the *Fermi* mission, providing a deep and uniform all-sky survey. It contains 514 sources, of which ~76% are statistically associated with active galactic nuclei (AGN), ~11% are sources of Galactic nature (pulsars, supernova remnants, and pulsar wind nebulae), while ~13% remain unassociated. Various observational campaigns were dedicated to searching for the low-frequency counterpart of the unassociated γ-ray sources (UGS) detected by *Fermi* (Nori et al. 2014; Massaro et al. 2013b; Giroletti et al. 2016). Recently, Schinzel et al. (2015) found 76 new low-frequency associations of γ-ray sources between 5 and 9 GHz

Table 1. Observations details.

Observing date	Experiment code	Stations log
2013 Dec. 9	S6340A	No FD
2013 Oct. 3	S6340B	No LA
2013 Oct. 4	S6340C	No LA
2013 Sep. 30	S6340D	No LA
2013 Nov. 22	S6340E	No FD
2013 Dec. 7	S6340F	No FD
2015 Jul. 10	S6340G	No PT
2015 Dec. 8	S6340H	–

Notes. Station codes: FD – Fort Davis, LA – Los Alamos, PT – Pie Town.

by detecting parsec-scale emission through Very Long Baseline Interferometric (VLBI) observations.

We are now investigating 1FHL sources at $\delta > 0°$ with the use of high angular resolution VLBI radio observations. There are several goals of this project: supporting the proposed blazar associations by revealing a compact high brightness temperature radio core; searching for new counterparts for UGS; increasing the size of the population of $E > 10$ GeV sources with high angular resolution observations; and exploring the existence of a correlation between VLBI and $E > 10$ GeV emission on a sample that is as large and unbiased as possible.

In this paper we present the first results of this project. From the whole 1FHL catalog we extracted a sample of 269 sources in the northern sky with a radio counterpart in the NRAO VLA Sky Survey (NVSS, Condon et al. 1998) within the 95% confidence radius (r95) by using TOPCAT software (Taylor 2005). We call this the 1FHL-n sample. For 185 out of these 269 sources Very Long Baseline Array (VLBA) archival observations are already available. Eighty-four sources (~31%) have never been observed with the VLBA, and 21 of them are UGS. We focus our attention on this these 84 1FHL sources (see Table A.1). For the sources with an association we aim to confirm their low-frequency association and to study their parsec scale properties. For the UGS we want to investigate their nature, possibly detecting a compact radio source associated with them.

The paper is organized as follows: in Sect. 2 we present the observations and data reduction procedures; we show the results in Sect. 3; we discuss and summarize the results in Sect. 4 and in Sect. 5, respectively. In a following paper, we will present a detailed statistical analysis of the entire 1FHL sample, based on new and archival data.

Throughout the paper, we use a ΛCDM cosmology with $h = 0.71$, $\Omega_m = 0.27$, and $\Omega_\Lambda = 0.73$ (Komatsu et al. 2011). The radio spectral index is defined such that $S(\nu) \propto \nu^{-\alpha}$ and the γ-ray photon index Γ such that $dN_{photon}/dE \propto E^{-\Gamma}$.

2. Observations and data reduction

We performed the VLBA observations between 2013 September 30 and December 7, and two additional observing epochs between 2015 July 10 and December 8. We divided the sample into eight observing blocks (Table 1). The observations were carried out at a central frequency of 5 GHz in full polarization; the total bandwidth of 256 MHz was divided into eight 32 MHz sub-bands in each polarization, with a recording rate of 2 Gbps. Observations were carried out in phase reference mode; the duty cycle of 5 min (4 min on target and 1 min on calibrator) was repeated six times, resulting in a net observing time of ~24 min per source. The total observing time for this project is 48 h. As shown in Table 1, during some observing epoch some antennas did not work properly because of technical problems.

Even if the angular resolution at $E > 10$ GeV (<0.15°) is lower than at lower γ-ray energies (<3.5° at $E > 100$ MeV), it still is much higher than the typical field of view of VLBI observations (milliarcsecond scale). Moreover, there are 18 sources for which there is not a single well-identified radio counterpart, but rather a set of a few possible candidates (between 2 and 5). For these sources we exploit the capability of the DiFX correlator (Deller et al. 2011) to correlate the data at multiple phase centers, one for each candidate radio counterpart. Thanks to this feature it is possible to observe all of the radio sources within the r95 region with one single pointing. However, some of them are located at a distance from the pointing center that is comparable to the 25 m single-dish primary beam at 5 GHz (~8 arcmin).

We carried out a full calibration by using the software package Astronomical Image Processing System (AIPS, Greisen 2003) with the following steps: phase calibration by applying ionospheric and Earth orientation parameters correction; amplitude calibration based on gain curves and measured system temperatures; parallactic angle correction; removal of residual instrumental phase and delay offset by using the pulse-cal tones table; global fringe fitting on all of the calibrator sources; and transfer of the solutions to the targets.

After this, we split the phase-referenced calibrated visibility data by averaging data in frequency within each sub-band, but not across IFs, and without any time average (the correlator integration time was 4 s). This provided a nominal field of view of 6.2 arcsec. With these single-source datasets, we started the editing and imaging process in DIFMAP (Shepherd 1997). Since the phase tracking centers were based on NVSS observations, which for faint sources can be as inaccurate as a few arcseconds, we often had to image wide sky regions before finding a significant source in the image plane. We determined the accurate positions and shift from the phase tracking center for all of the detected sources (see Table A.1). We then went back to the multi file in AIPS and for each source we corrected the position by using the task CLCOR.

After this calibration procedure, for the six sources (1FHL J0338.4+1304, 1FHL J0516.4+7351, 1FHL J1244.9+5708, 1FHL J1315.0+2346, 1FHL J1942.8+1034, and 1FHL J2223.4+0104) whose calibrators have some extended structures, we imaged the calibrator in DIFMAP and we produced a model that we use in AIPS for two self-calibration cycles with the task CALIB. The source 1FHL J0930.4+8611 is quite strong ($S > 200$ mJy/beam) and we performed a global fringe-fit on the source itself.

After splitting the single-source visibility datasets, we started a final cycle of imaging and self calibration in AIPS, obtaining for each source the peak flux density and the deconvolved angular size by using the task JMFIT. Finally, for the sources with a significant offset from the pointing center, we corrected for primary beam attenuation by using the widefield VLBI calculator[1].

For 11 sources (marked with an asterisk in Table A.1) we observed the NVSS source, which is closer to the 1FHL source centroid but is not coincident with the proposed low-frequency association in the 1FHL. For this reason we exclude these 11 sources from our analysis. We also exclude the supernova

[1] http://www.atnf.csiro.au/people/Emil.Lenc/Calculators/wfcalc.php

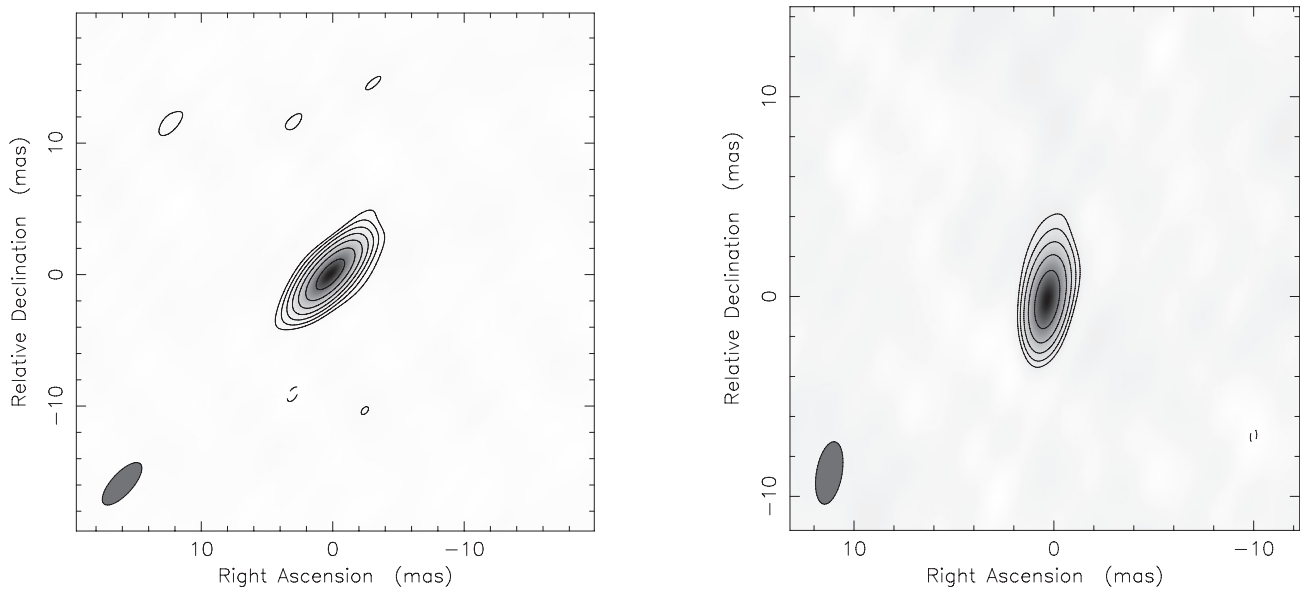

Fig. 1. 5 GHz VLBA image of the radio counterparts of the γ-ray sources 1FHL J0043.7+3425 (*left panel*), classified as a FSRQ, and 1FHL J0648.9+1516 (*right panel*), classified as a BL Lac. The beam size is 1.6 mas × 4.1 mas and 1.3 mas × 3.2 mas, respectively. Levels are drawn at $(-1, 1, 2, 4...)\times$ the lowest contour (i.e., at 1.2 mJy/beam for the source 1FHL J0043.7+3425 and at 1.4 mJy/beam for the source 1FHL J0648.9+1516) in steps of 2. The noise level is 0.31 mJy and 0.37 mJy, respectively.

remnant source 1FHL J1911.0+0905 and the final sample discussed in this paper consists of 72 sources.

3. Results

3.1. VLBI properties and detection rate

We detect radio emission on VLBI scales for 67/72 sources, which corresponds to an overall detection rate of 93%. For blazars the detection rate is 100% (51/51), while for the UGS it is 76% (16/21). The significance level for the detection of these sources is always $\gg 5\sigma$. The VLBI coordinates, the 10−500 GeV energy flux (S_γ), the 1.4 GHz NVSS flux density ($S_{1.4,\mathrm{NVSS}}$), the 5 GHz VLBA flux density ($S_{5,\mathrm{VLBI}}$), and the brightness temperature of the detected sources are listed in Table A.2.

In Fig. 1 we show an example of 5 GHz images of the FSRQ source 1FHL J0043.7+3425 (left panel), and the BL Lac source 1FHL J0648.9+1516 (right panel), which are representative of the global dataset. For these 67 sources we reveal for the first time a VLBI compact structure. The detection is also confirmed by a visual inspection of the visibility data.

In five sources (1FHL J0338.4+1304, 1FHL J1315.0+2346, 1FHL J1809.3+2040, 1FHL J1942.8+1034 and 1FHL J2223.4+0104) we reveal some extended structures close to the compact region. Examples of extended sources are shown in Fig. 2. We used the AIPS task JMFIT to fit the brightness distribution of each extended source in the image plane with two elliptical Gaussian components. In Table 2 we list the full widths at half maximum (FWHM) of the major and minor axes of the deconvolved elliptical Gaussian component measured in mas.

3.2. Flux density distribution

The distribution of $S_{1.4,\mathrm{NVSS}}$ of the newly VLBA detected sources is shown in the top panel of Fig. 3 (red solid line), which has a median value of 40.6 mJy. In the middle panel of Fig. 3 we show the $S_{5,\mathrm{VLBI}}$ distribution (red solid line), which has a median value of 16.3 mJy. In both panels we also show separately the distribution of flux densities for the blazars (green dashed line) and for the UGS (blue dashed line). We note that for the UGS the median values for both $S_{1.4,\mathrm{NVSS}}$ (31.2 mJy) and $S_{5,\mathrm{VLBI}}$ (8.9 mJy) are lower than for the blazars (median values of 47.3 mJy and 19.5 mJy for $S_{1.4,\mathrm{NVSS}}$ and $S_{5,\mathrm{VLBI}}$, respectively).

In the bottom panel of Fig. 3 we show the distribution of the logarithm of the ratio between the flux density on parsec scale ($S_{5,\mathrm{VLBI}}$) and on kiloparsec scale ($S_{1.4,\mathrm{NVSS}}$). The distribution peaks at ∼0.5, indicating that for most sources there is a considerable amount of radio emission on intermediate scales between the parsec and kiloparsec scales.

By an inspection of both NVSS and VLBI flux densities, it emerges that there are some interesting sources. In ∼10% of the sources the ratio $S_{5,\mathrm{VLBI}}/S_{1.4,\mathrm{NVSS}}$ is significantly higher than 1, as in the case of the UGS 1FHL J0307.4+4915, with $S_{5,\mathrm{VLBI}} = 300 \pm 30$ mJy, while $S_{1.4,\mathrm{NVSS}}$ is 56.0 ± 1.7 mJy. At the other end of the distribution there are sources for which the ratio $S_{5,\mathrm{VLBI}}/S_{1.4,\mathrm{NVSS}}$ is significantly lower than 1. For example, for the sources 1FHL J0333.6+2918, 1FHL J0334.0+6539, 1FHL J0601.0+3838, and 1FHL J2127.8+3614, the ratio $S_{5,\mathrm{VLBI}}/S_{1.4,\mathrm{NVSS}}$ is between 0.1 and 0.2.

The immediate interpretation is that the sources with $S_{1.4,\mathrm{NVSS}} \gg S_{5,\mathrm{VLBI}}$ have extended emission (on arcsecond scale), while in the case of $S_{5,\mathrm{VLBI}} \gg S_{1.4,\mathrm{NVSS}}$ some degree of variability could be responsible of the higher observed VLBI flux density. However, it is important to stress that we are comparing non-concurrent observations at different spatial scales and at different frequencies.

3.3. High energy properties

The distribution of 1FHL S_γ for the detected sources is presented in the left panel of Fig. 4 (red solid line), showing a median value of 4.8×10^{-12} erg cm^{-2} s^{-1}. In particular, blazars (green dashed lines) and the UGS (blue dashed lines) have median values of 5.1×10^{-12} and 4.5×10^{-12} erg cm^{-2} s^{-1}, respectively.

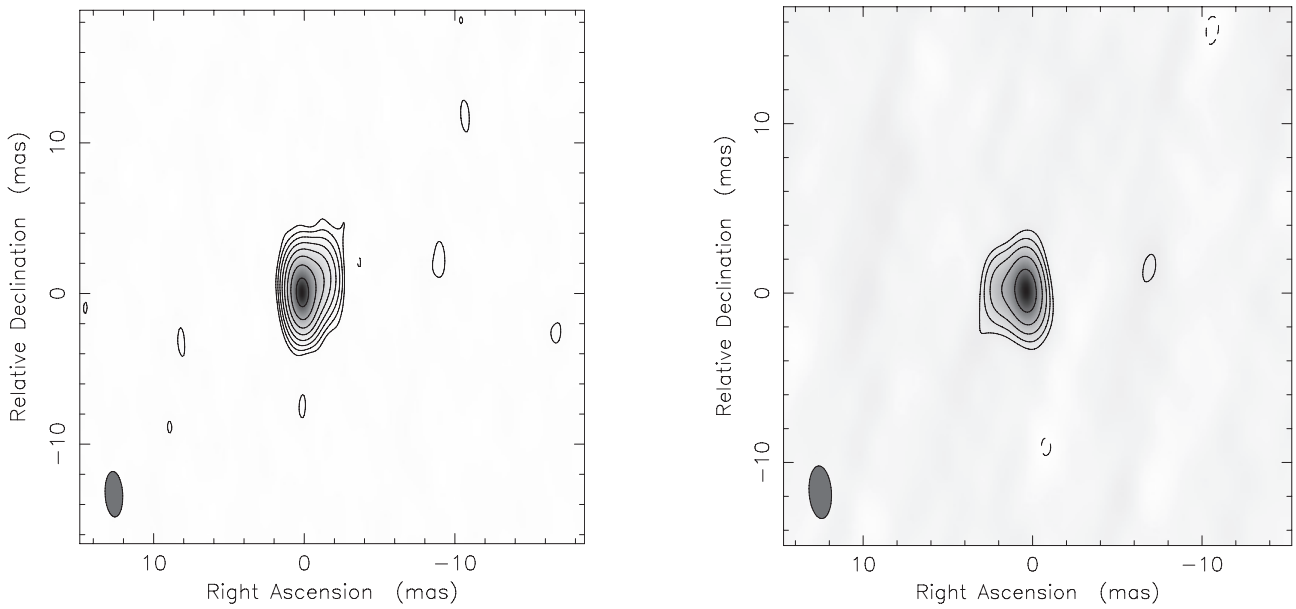

Fig. 2. 5 GHz VLBA image of the radio counterparts of the γ-ray sources 1FHL J1315.0+2346 (*left panel*), classified as a BL Lac, and 1FHL J1942.8+1034 (*right panel*), classified as an active galaxy of uncertain type. The beam size is 1.2 mas × 3.0 mas and 1.3 mas × 3.1 mas, respectively. Levels are drawn at $(-1, 1, 2, 4...)\times$ the lowest contour (i.e., at 0.4 mJy/beam for the source 1FHL J1315.0+2346 and at 2.0 mJy/beam for the source 1FHL J1942.8+1034) in steps of 2. The noise level is 0.12 mJy and 0.50 mJy, respectively.

Table 2. Modelfit details for the extended sources.

1FHL name	Component	S[a] mJy	σ_S mJy	a^b mas	b^b mas	$D_{\rm core}{}^c$ mas	Orientation[d] deg
J0338.4+1304	Core	6.33	0.29	0.80	0.00	–	–
	C1	3.94	0.29	0.39	0.00	1.46	−28.0
J1315.0+2346	Core	51.27	0.12	0.22	0.00	–	–
	C1	30.57	0.33	1.76	0.72	0.50	−49.1
J1809.3+2040	Core	26.82	0.20	0.67	0.00	–	–
	C1	14.48	0.72	5.02	1.46	1.36	−18.7
J1942.8+1034	Core	53.30	0.78	0.73	0.52	–	–
	C1	13.07	0.41	1.06	0.00	0.72	89.0
J2223.4+0104	Core	6.80	0.24	0.96	0.30	–	–
	C1	3.41	0.13	0.88	0.00	1.35	157.4

Notes. [(a)] Fitted core flux density at 5 GHz. [(b)] a and b are the nominal FWHM of the major and minor axes of the deconvolved elliptical Gaussian component measured in mas. [(c)] Distance from the core of the C1 Gaussian component. [(d)] Orientation of the extended structure. Angles are measured from north through east.

The photon index distribution is shown in the right panel of Fig. 4, and has a median value of 2.3 both for the blazars (green dashed lines) and the UGS (blue dashed lines).

3.4. Proposed counterparts for unassociated sources

For 16 out of the 21 UGS studied in this paper, we detect radio emission on VLBI scales and we propose a possible radio NVSS counterpart. By using the approach proposed by Schinzel et al. (2015), we determine the likelihood ratio for the association of each of the detected UGS. Schinzel et al. (2015) propose a likelihood ratio threshold value of 8, chosen from the distribution of the obtained values of their full sample, to claim the association of the γ-ray source with the proposed radio counterpart. For all of the detected UGS in the present work but two (1FHL J0605.4+2726 and 1FHL J1212.2+2318), the likelihood ratio of their association is higher than 8. The detected UGS, along with further details about other γ-ray associations, are listed in Table 3.

We note that 8 out of the 16 detected UGS in our sample are included in the all-sky radio survey, between 5 and 9 GHz, of sky areas surrounding all of the second *Fermi*-LAT catalog (2FGL, Nolan et al. 2012) UGS by Schinzel et al. (2015). Our proposed low-frequency associations always match those proposed by Schinzel et al. (2015) and by using their 7 GHz VLBA observations we obtain the spectral index values between 5 and 7 GHz (see Table 3).

For these eight 1FHL UGS included in the 2FGL catalog, our proposed low-frequency counterparts are in agreement with those proposed in other works which make use of complementary association methods based on the analysis of their multiwavelength (MWL) properties, such as the investigation of infrared colors and the low-frequency spectral index (Massaro et al. 2013a,b, 2014, 2015). Our proposed counterparts

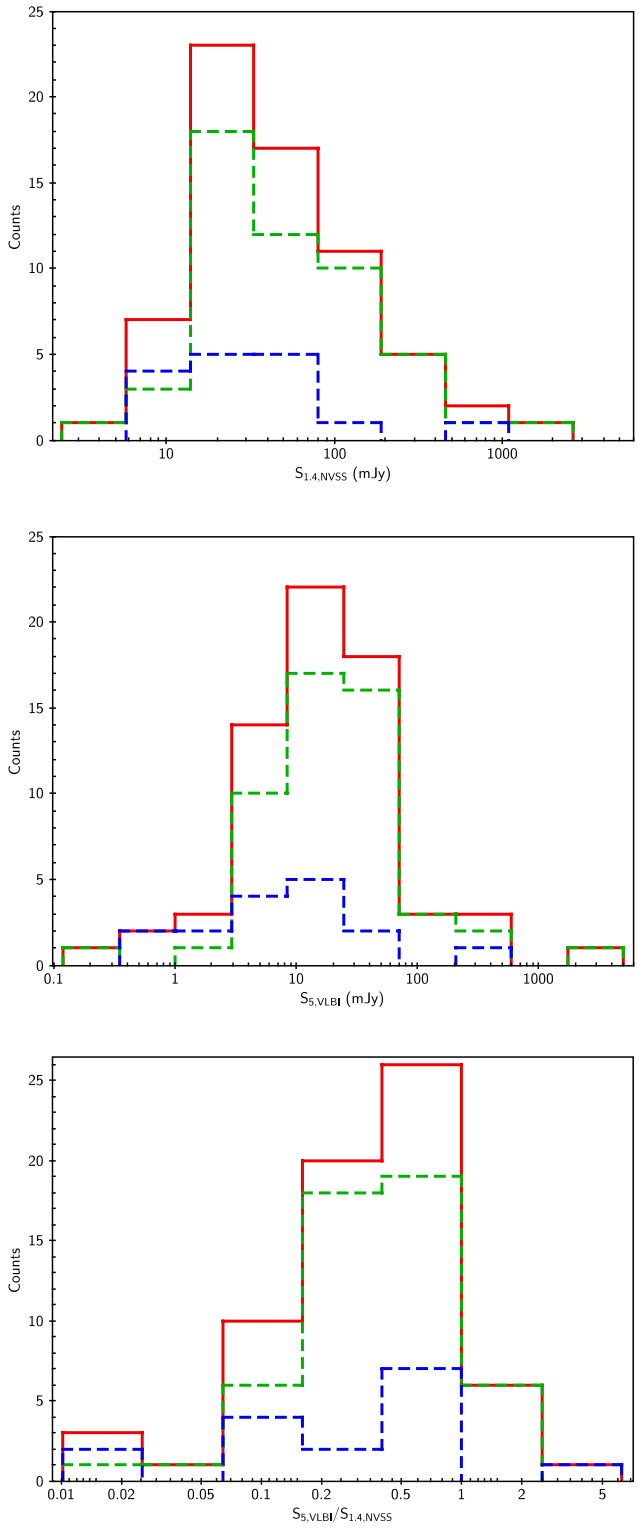

Fig. 3. Flux density distribution for the detected sources. *Top panel*: 1.4 GHz NVSS flux density distribution; *middle panel*: 5 GHz VLBA flux density distribution; *bottom panel*: distribution of the ratio between the 5 GHz VLBA and the 1.4 GHz NVSS flux densities. Solid red line: All sources; green dashed line: Blazars; blue dashed line: UGS.

for the sources 1FHL J0644.2+6036, 1FHL J1223.3+7953, and 1FHL J0601.0+3838 are compatible with the X-ray associations proposed by Landi et al. (2015) and Paggi et al. (2013), as indicated in the notes in Table 3.

In Table 3, we also list the sources 1FHL J0332.1+6307, 1FHL J0338.4+1304, 1FHL J0425.3+6320, 1FHL J0601.0+3838, 1FHL J0650.4+2056, 1FHL J1841.1+2914, 1FHL J2002.6+6303, and 1FHL J2004.7+7003, for which new low-frequency counterparts are proposed in the 3FGL catalog. For the source 1FHL J0307.4+4915 a new low-frequency counterpart is now proposed in the second catalog of hard *Fermi*-LAT sources (2FHL, Ackermann et al. 2016). All of these new associations are coincident with those proposed in this work.

For the sources 1FHL J0053.9+4030 and 1FHL J1619.8+7540 we propose, for the first time, a new low-frequency association. We note that the source 1FHL J0053.9+4030 is one of the faintest sources ($S_{\rm VLBI} \sim 5$ mJy) in our sample and it is not included in any other *Fermi* catalog. For the sources 1FHL J0605.4+2726 and 1FHL J1212.2+2318, which are not included in any other *Fermi* catalog, we propose a new low-frequency counterpart, but for their association we find a likelihood ratio lower than 8. In both cases the proposed radio counterpart is located very close to the edge of the 1FHL error ellipse.

Among the five undetected UGS, the sources 1FHL J1406.4+1646 and 1FHL J0828.9+0902 are now associated in the 3FGL with sources not included among our observed phase centers; the source 1FHL J0625.9+0002 is included in the 3FGL and classified as UGS; the sources 1FHL J0625.9+0002 and 1FHL J0432.2+5555 are not included in any other *Fermi* catalog.

3.5. Measurements of the brightness temperature

The high resolution of VLBI observations allows a direct measurement of the brightness temperature of a source. However, because blazar jets are highly relativistic, and therefore Doppler boosted, it is difficult to measure the intrinsic brightness temperature ($T_{\rm B}^{\rm int}$). What we measure is the observed brightness temperature ($T_{\rm B}^{\rm obs}$), which is linked to $T_{\rm B}^{\rm int}$ by the relation $T_{\rm B}^{\rm obs} = \delta^{3+\alpha} \cdot T_{\rm B}^{\rm int}$, where δ is the Doppler factor and α is the spectral index.

By fitting the brightness distribution of each source in the image plane with elliptical Gaussian components, and assuming $\alpha = 0$, we determine $T_B^{\rm obs}$ for each source with the equation (Piner et al. 1999; Tingay et al. 1998)

$$T_{\rm B}^{\rm obs} = 1.22 \times 10^{12} \times \frac{S_{\rm core}(1+z)}{abv^2},$$

where $S_{\rm core}$ corresponds to the fitted core flux density at 5 GHz measured in Jy, a and b are the FWHM of the major and minor axes of the elliptical Gaussian core component measured in mas, z is the redshift, and ν is the observing frequency in GHz.

For the sources without any redshift estimation we assume $z = 0.2$, which corresponds to the median redshift value of 1FHL BL Lac objects. We note that for some sources the radio core is only slightly resolved or is unresolved (i.e., less than half of the beam size).

For those sources we determine measurements as upper limits to a and b based on the Gaussian deconvolved size reported by the AIPS task JMFIT (Greisen 2003). When a nominal value is provided we use it as measurement, when only a maximum value is reported we treat it as an upper limit, resulting in a $T_{\rm B}^{\rm obs}$ lower limit. In a few cases, also the maximum value reported by JMFIT is 0; for these sources we conservatively set the upper limit to the minimum size value found among the other sources.

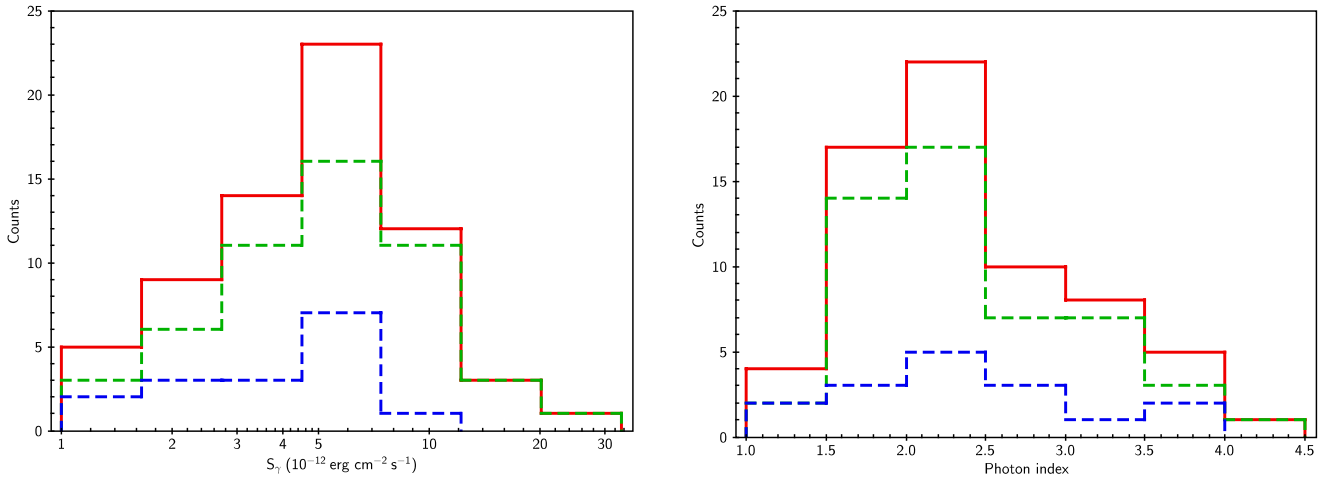

Fig. 4. Distribution of γ-ray energy flux (*left panel*) and photon index (*right panel*) above 10 GeV for the detected sources. Solid red line: all sources; green dashed line: Blazars; blue dashed line: UGS.

Table 3. Details of the 16 detected UGS.

1FHL name	NVSS assoc	2FGL name	3FGL name	2FHL name	α^a	σ_α	Notes
J0053.9+4030	J005330+403015	–	–	–	–	–	–
J0307.4+4915	J030727+491510	J0307.4+4915	J0307.3+4916	J0307.4+4917	−0.3	0.4	1,2,3
J0332.1+6307	J033153+630814	J0332.1+6309	J0332.0+6308	–	−1.0	0.4	1,2,3
J0338.4+1304	J033829+130215	J0338.2+1306	J0338.5+1303	–	−2.3	0.4	2,3
J0425.3+6320	J042524+632005	–	J0425.2+6319	J0425.1+6317	–	–	–
J0601.0+3838	J060102+383828	J0600.9+3839	J0601.0+3837	J0601.0+3837	−0.2	0.4	1,2,3,5,6
J0605.4+2726	J060501+272456	–	–	–	–	–	–
J0644.2+6036	J064435+603849	J0644.6+6034	J0644.6+6035	–	−2.7	0.4	1,3,4,5
J0650.4+2056	J065035+205556	–	J0650.5+2055	J0650.5+2056	–	–	–
J1212.2+2318	J121238+231110	–	–	–	–	–	–
J1223.3+7953	J122358+795329	J1223.3+7954	J1222.7+7952	–	−0.7	0.4	1,2,3,5,7
J1548.3+1455	J154824+145702	J1548.3+1453	J1548.4+1455	–	−1.1	0.4	2,3,5
J1619.8+7540	J161913+753753	–	J1619.1+7538	–	–	–	–
J1841.1+2914	J184121+290945	–	J1841.2+2910	–	–	–	–
J2002.6+6303	J200244+630230	–	J2002.7+6303	–	–	–	–
J2004.7+7003	J200506+700440	J2004.6+7004	J2004.8+7003	–	−2.2	0.4	2,3,4,5

Notes. $^{(a)}$ Spectral index calculated by using the 5 GHz VLBA flux densities of the present work together with the 7 GHz VLBA flux densities provided by Schinzel et al. (2015). (1) Association also proposed by Massaro et al. (2013a). (2) Association also proposed by Massaro et al. (2015). (3) Association also proposed by Schinzel et al. (2015). (4) Association also proposed by Massaro et al. (2013b). (5) Association also proposed by Massaro et al. (2014). (6) Association also proposed by Paggi et al. (2013). (7) Association also proposed by Landi et al. (2015).

The resulting brightness temperature values are reported in Table A.2. For the 36 sources whose radio core is resolved, the average $T_{\rm B}^{\rm obs}$ is on the order of 2×10^{10} K, which is close to the expected value for equipartition. Only five sources have $T_{\rm B}^{\rm obs}$ varying in the range 7×10^{10}–1×10^{11} K.

4. Discussion

4.1. General characterization of the observed sample

The 1FHL catalog provides us, for the first time, with a deep, large and unbiased sample of sources detected in the energy range 10–500 GeV. It fills the gap existing between the HE and VHE regimes, represented by 3FGL and TeVCat[2], respectively.

An important step on the basis of the analysis and interpretation of the physical properties of these sources is the investigation and comparison of the multifrequency properties for the entire catalog. However, such a study cannot be carried out while neglecting a significant fraction of the sample, i.e., the 84 sources without VLBI data presented here. These 84 sources do not represent a random 1FHL subsample. Their 1.4 GHz NVSS radio flux density distribution is significantly different with respect to the other sources belonging to the 1FHL-n sample (Fig. 5). A KS-test provides a probability of the two distributions being drawn from the same population of $\sim 2 \times 10^{-12}$. Another peculiarity of our sample is that 61% of the selected AGNs are of HSP type, while in the complementary sample of 1FHL-n sources already observed with VLBI the fraction of HSPs is 40%. This occurs mainly because we are targeting a 1FHL subsample of sources with the faintest radio flux densities, in agreement with the blazar sequence trend (e.g., Fossati et al. 1998; Ghisellini et al. 1998). Moreover, the fraction of HSP objects without a known redshift in our sample is 65%, while in the 1FHL-n they represent 42%. Finally, we note that while 10% of 1FHL sources at Dec > 0° are classified as UGS, in our sample the fraction of UGS is 29%. We are targeting 88% (21/24) of

[2] http://tevcat.uchicago.edu/

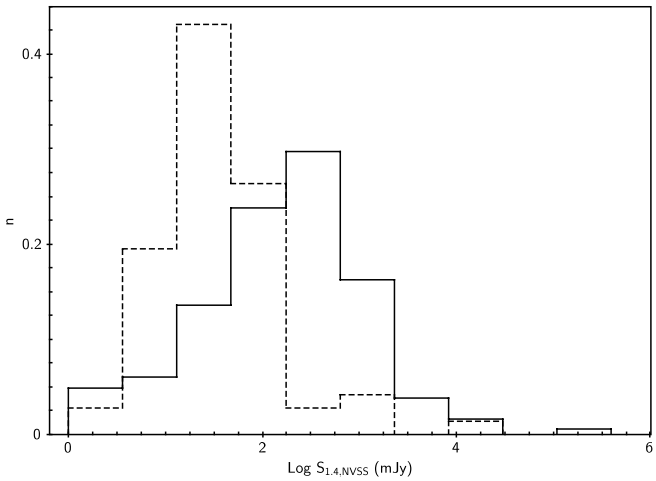

Fig. 5. Histogram of the NVSS flux density distribution for VLBA observed sources (solid line) and unobserved sources (dashed line) in our sample.

the 1FHL UGS in the northern sky with at least one NVSS counterpart within the r95. Therefore, we are not only completing the VLBI data collection for the whole sample of hard γ-ray sources, but we are also characterizing an unexplored population.

4.2. VLBI properties and unassociated sources

The vast majority of the detected sources in our sample are radio weak (with flux densities of a few mJy). For all of the detected sources we reveal a VLBI compact component and we confirm their blazar nature. This finding provides an independent validation of other association methods based on the analysis of their multiwavelength properties, such as the investigation of infrared colors, the low-frequency spectral index, and the X-ray association (e.g., D'Abrusco et al. 2013; Massaro et al. 2013a; Nori et al. 2014; Landi et al. 2015).

It is interesting to note that the detection rate of compact components for the UGS is remarkably high (76%). This is a first indication that the nature of the UGS is similar to the associated sources, i.e., they are mostly blazars. This hypothesis is supported by the fact that both $S_{1.4,\mathrm{NVSS}}$ and $S_{5,\mathrm{VLBI}}$ for the blazars and the UGS are distributed in a similar way (see Fig. 3). This also shows how much the NVSS survey is useful for a preselection of compact radio counterparts, and deeper Jansky very large array and Australia telescope compact array observations are only needed in special cases (Schinzel et al. 2015). However, the VLBI observations are necessary for the actual selection of the right association.

We note that for the UGS both the NVSS and VLBI flux densities are lower than for the associated sources (Fig. 3); therefore, they may be weaker blazars not yet identified. Moreover, for eight detected UGS we calculated the spectral index values between 5 and 7 GHz VLBA data, which are either flat or inverted, indicating the presence of a self-absorbed region. In particular for the source 1FHL J0644.2+6036 the spectral index is strongly inverted ($\alpha = -2.7$), exceeding the canonical value of -2.5 for a homogeneous synchrotron emission region. This is an indication that variability is occurring in this source. A clear example of flux density variability is provided by the source 1FHL J0307.4+4915, for which we find $S_{5,\mathrm{VLBI}} = 300 \pm 30$ mJy, while $S_{1.4,\mathrm{NVSS}}$ is 56.0 ± 1.7 mJy.

4.3. Brightness temperature

For the detected sources we estimated the VLBI core brightness temperature, which can be used to distinguish between the physical processes occurring in the source. In a synchrotron source there are two main physical mechanisms which can limit the intrinsic brightness temperature. One is the inverse Compton (IC) process, which limits $T_{\mathrm{B}}^{\mathrm{int}}$ in the range $\sim 5 \times 10^{11}$–10^{12} K (Kellermann & Pauliny-Toth 1969). When this limit is exceeded the IC process leads to rapid and catastrophic electron energy losses. The second relevant physical mechanism is the energy equipartition between particles and magnetic field which limits the $T_{\mathrm{B}}^{\mathrm{int}}$ in the range $\sim 5 \times 10^{10}$–10^{11} K (Readhead 1994).

For the vast majority of the sources in our sample whose cores are resolved we obtain brightness temperature values on the order of 2×10^{10} K, which is close to the expected value for equipartition. Therefore, we expect the energy to be almost equally stored in the magnetic field and in the radiating particles. These values are consistent with the typical HSP blazar $T_{\mathrm{B}}^{\mathrm{obs}}$, and are in agreement with the values obtained in other works (e.g., Piner et al. 2010; Lico et al. 2012, 2014; Piner & Edwards 2014). From these $T_{\mathrm{B}}^{\mathrm{obs}}$ values no high Doppler factors are required and there is no evidence of a strong beaming. However, we note that at 5 GHz we are observing these sources in their self-absorbed part of the synchrotron spectrum, therefore the flux densities and the brightness temperatures may be underestimated.

5. Summary and conclusions

In the present work we targeted and characterized the 1FHL sources in the northern sky with the faintest radio flux densities; these sources represent an important extension to an unexplored region of the parameter space, and are essential to obtain a sample that is as large and unbiased as possible to explore the possible correlation between radio VLBI and $E > 10$ GeV emission.

- For all of the detected sources we reveal a compact high brightness temperature VLBI radio core and we confirm their blazar nature. The vast majority are radio weak sources, with a VLBI flux density median value of 16.3 mJy, consistent with the predictions of the blazar sequence (e.g., Fossati et al. 1998; Ghisellini et al. 1998).
- Thanks to the new VLBI observations we propose new low-frequency counterparts for 16 1FHL UGS. We note that for 12 out of the 16 detected UGS our proposed low-frequency counterparts are in agreement with those proposed by using indirect and complementary association methods based on the analysis of their MWL properties, and with those included in the 2FHL and 3FGL catalogs. For the remaining four 1FHL UGS we propose a low-frequency counterpart for the first time.
- For the sources whose radio core is resolved we obtain brightness temperature values on the order of 2×10^{10} K, which are close to the value expected for the equipartition of energy between particles and magnetic field. Therefore, there is no evidence of a strong beaming and no high Doppler factor values are required. This result increases the statistical significance of the similar brightness temperature values obtained for other HSP sources (e.g., Giroletti et al. 2004; Piner & Edwards 2014).

Ackermann et al. (2011) found a strong and significant correlation between radio and γ rays in the 0.1–100 GeV energy range for blazars belonging to the first catalog of AGNs detected by

Fermi (1LAC, Abdo et al. 2010b); however, no systematic investigation for the existence of a possible correlation between radio and VHE γ rays has been made. The main reason is that at VHE there is no homogeneous, deep and large survey that allows us to perform a similar correlation analysis; the IACTs have small field of view and they mainly observe in pointing mode. All of these limitations will be overcome in the coming years thanks to the new generation Cherenkov Telescope Array (CTA, Dubus et al. 2013). The investigation in the VHE domain is important because it provides us with details about the blazar sequence (i.e., the anti-correlation between the synchrotron luminosity and the SED peak frequency (Fossati et al. 1998)), and the interaction of VHE photons with the EBL (e.g., Ackermann et al. 2012).

In a following paper, by using the VLBI flux densities presented in this work complemented by VLBI archival observations, we will explore and quantify the possible radio-VHE correlation for the 1FHL AGN sample.

Acknowledgements. We thank Leonid Petrov for his support and the fruitful discussions. We thank the anonymous referee for the helpful comments and discussions which improved the manuscript. This work is based on observations obtained through the S6340 VLBA project, in the framework of the *Fermi*-NRAO cooperative agreement. The VLBA makes use of the Swinburne University of Technology software correlator, developed as part of the Australian Major National Research Facilities Programme and operated under licence (Deller et al. 2011). We acknowledge financial contribution from grant PRIN-INAF-2011 and PRIN-INAF-2014. This research has made use of NASA's Astrophysics Data System, of the VizieR catalog access tool, CDS, Strasbourg, France and the TOPCAT software (Taylor 2005). The National Radio Astronomy Observatory is a facility of the National Science Foundation operated under cooperative agreement by Associated Universities, Inc. For this paper we made use of the NASA/IPAC Extragalactic Database NED, which is operated by the JPL, Californian Institute of Technology, under contract with the National Aeronautics and Space Administration. The *Fermi*-LAT Collaboration acknowledges support for LAT development, operation, and data analysis from NASA and DOE (United States), CEA/Irfu and IN2P3/CNRS (France), ASI and INFN (Italy), MEXT, KEK, and JAXA (Japan), and the K. A. Wallenberg Foundation, the Swedish Research Council, and the National Space Board (Sweden). Science analysis support in the operations phase from INAF (Italy) and CNES (France) is also gratefully acknowledged.

References

Abdo, A. A., Ackermann, M., Agudo, I., et al. 2010a, ApJ, 716, 30
Abdo, A. A., Ackermann, M., Ajello, M., et al. 2010b, ApJ, 715, 429
Acero, F., Ackermann, M., Ajello, M., et al. 2015, ApJS, 218, 23
Ackermann, M., Ajello, M., Allafort, A., et al. 2011, ApJ, 741, 30
Ackermann, M., Ajello, M., Allafort, A., et al. 2012, Science, 338, 1190
Ackermann, M., Ajello, M., Allafort, A., et al. 2013, ApJS, 209, 34
Ackermann, M., Ajello, M., Atwood, W. B., et al. 2015, ApJ, 810, 14
Ackermann, M., Ajello, M., Atwood, W. B., et al. 2016, ApJS, 222, 5
Condon, J. J., Cotton, W. D., Greisen, E. W., et al. 1998, AJ, 115, 1693
D'Abrusco, R., Massaro, F., Paggi, A., et al. 2013, ApJS, 206, 12
Deller, A. T., Brisken, W. F., Phillips, C. J., et al. 2011, PASP, 123, 275
Dubus, G., Contreras, J. L., Funk, S., et al. 2013, Astropart. Phys., 43, 317
Fossati, G., Maraschi, L., Celotti, A., Comastri, A., & Ghisellini, G. 1998, MNRAS, 299, 433
Ghisellini, G., Celotti, A., Fossati, G., Maraschi, L., & Comastri, A. 1998, MNRAS, 301, 451
Giroletti, M., Giovannini, G., Taylor, G. B., & Falomo, R. 2004, ApJ, 613, 752
Giroletti, M., Massaro, F., D'Abrusco, R., et al. 2016, A&A, 588, A141
Greisen, E. W. 2003, Astrophys. Space Sci. Lib, 285, 109
Kellermann, K. I., & Pauliny-Toth, I. I. K. 1969, ApJ, 155, L71
Komatsu, E., Smith, K. M., Dunkley, J., et al. 2011, ApJS, 192, 18
Landi, R., Bassani, L., Stephen, J. B., et al. 2015, A&A, 581, A57
Lico, R., Giroletti, M., Orienti, M., et al. 2012, A&A, 545, A117
Lico, R., Giroletti, M., Orienti, M., et al. 2014, A&A, 571, A54
Massaro, F., D'Abrusco, R., Giroletti, M., et al. 2013a, ApJS, 207, 4
Massaro, F., D'Abrusco, R., Paggi, A., et al. 2013b, ApJS, 206, 13
Massaro, F., D'Abrusco, R., Paggi, A., et al. 2014, ApJS, submitted [arXiv:1404.5960]
Massaro, F., Landoni, M., D'Abrusco, R., et al. 2015, A&A, 575, A124
Nolan, P. L., Abdo, A. A., Ackermann, M., et al. 2012, ApJS, 199, 31
Nori, M., Giroletti, M., Massaro, F., et al. 2014, ApJS, 212, 3
Paggi, A., Massaro, F., D'Abrusco, R., et al. 2013, ApJS, 209, 9
Piner, B. G., & Edwards, P. G. 2014, ApJ, 797, 25
Piner, B. G., Unwin, S. C., Wehrle, A. E., et al. 1999, ApJ, 525, 176
Piner, B. G., Pant, N., & Edwards, P. G. 2010, ApJ, 723, 1150
Readhead, A. C. S. 1994, ApJ, 426, 51
Schinzel, F. K., Petrov, L., Taylor, G. B., et al. 2015, ApJS, 217, 4
Shepherd, M. C. 1997, ASP Conf. Ser., 125, 77
Taylor, M. B. 2005, Astronomical Data Analysis Software and Systems XIV, ASP Conf. Ser., 347, 29
Tingay, S. J., Murphy, D. W., Lovell, J. E. J., et al. 1998, ApJ, 497, 594

Appendix A: Additional tables

Table A.1. Sample source details.

IFHL name[a]	Assoc	Class	z	RA[b] h:m:s	Dec[b] d:m:s.	Shift RA mas	Shift Dec mas	Detection	Exp. code
J0007.7+4709	MG4 J000800+4712	bzb	0.28	00:07:45.22	+47:11:31.0	−135.6	31.4	Y	S6340H
J0009.2+5032	NVSS J000922+503028	bzb	–	00:09:22.53	+50:30:28.9	−2190.5	52.0	Y	S6340A
J0037.8+1238	NVSS J003750+123818	bzb	0.09	00:37:50.85	+12:38:18.8	−443.0	−1079.5	Y	S6340A
J0040.3+4049	1ES 0037+405	bzb	–	00:40:13.50	+40:50:05.4	−3552.4	704.4	Y	S6340B
J0043.7+3425	GB6 J0043+3426	bzq	0.97	00:43:48.86	+34:26:26.3	210.0	206.5	Y	S6340A
J0053.9+4030	UGS	–	–	00:53:31.76	+40:27:21.5	−867.8	−3859.8	Y	S6340H
J0103.4+5336	1RXS J010325.9+533721	agu	–	01:03:26.08	+53:37:12.1	1085.0	−1179.0	Y	S6340B
J0122.7+3425*	1ES 0120+340	bzb	0.27	01:22:38.81	+34:26:11.3	–	–	N	S6340B
J0131.3+6121	1RXS J013106.4+612035	agu	–	01:31:07.16	+61:20:33.0	−478.5	−368.0	Y	S6340B
J0134.4+2643	1RXS J013427.2+263846	agu	–	01:34:27.99	+26:38:42.5	−2759.0	−525.0	Y	S6340B
J0153.1+7515	BZB J0153+7517	bzb	–	01:53:07.26	+75:17:44.2	−459.5	1268.0	Y	S6340B
J0213.1+2246	MG3 J021252+2246	bzb	0.46	02:12:52.78	+22:44:55.1	−752.0	2858.0	Y	S6340B
J0241.3+6548	NVSS J024121+654311	agu	–	02:41:26.41	+65:45:47.7	−471.5	321.0	Y	S6340H
J0307.4+4915	UGS	–	–	03:07:27.06	+49:15:10.3	246.0	546.0	Y	S6340B
J0322.1+2337	MG3 J032201+2336	bzb	–	03:22:00.05	+23:36:10.0	1093.5	−1205.5	Y	S6340B
J0332.1+6307	UGS	–	–	03:31:53.76	+63:08:14.3	−1056.5	139.0	Y	S6340A
J0333.6+2918	TXS 0330+291	bzb	–	03:33:49.02	+29:16:31.6	214.0	51.0	Y	S6340A
J0334.0+6539	TXS 0329+654	bzb	–	03:33:56.74	+65:36:56.2	1.0	−1.5	Y	S6340A
J0338.4+1304	UGS	–	–	03:38:29.30	+13:02:15.0	305.0	−449.0	Y	S6340A
J0425.3+6320	UGS	–	–	04:25:24.77	+63:20:05.6	−3944.0	3918.5	Y	S6340B
J0425.4+5601	UGS	–	–	04:26:04.31	+56:03:39.6	–	–	N	S6340B
J0432.2+5555	UGS	–	–	04:32:02.39	+55:48:44.2	–	–	N	S6340H
J0515.9+1528	GB6 J0515+1527	bzb	–	05:15:47.41	+15:27:16.9	820.0	307.5	Y	S6340C
J0516.4+7351	GB6 J0516+7350	bzb	0.25	05:16:31.12	+73:51:08.8	−469.0	140.0	Y	S6340C
J0529.0+0937	GB6 J0529+0934	agu	–	05:29:02.57	+09:34:32.5	−724.5	4318.0	Y	S6340C
J0540.5+5822	GB6 J0540+5823	bzb	–	05:40:29.97	+58:23:39.5	−309.0	1048.0	Y	S6340C
J0601.0+3838	UGS	–	–	06:01:02.90	+38:38:28.8	362.0	−370.5	Y	S6340C
J0605.0+0001	GB6 J0604+0000	agu	–	06:04:58.43	+00:00:43.1	177.5	−254.5	Y	S6340C
J0605.4+2726	UGS	–	–	06:05:01.05	+27:24:56.3	−1216.5	−1138.0	Y	S6340C
J0606.6+4742*	CGRaBS J0607+4739	bzb	–	06:06:38.31	+47:41:47.4	–	–	N	S6340C
J0625.9+0002	UGS	–	–	06:26:12.88	+00:03:34.6	–	–	N	S6340C
J0644.2+6036	UGS	–	–	06:44:35.64	+60:38:49.8	−777.0	−1363.0	Y	S6340C
J0648.9+1516	VER J0648+152	bzb	0.18	06:48:47.63	+15:16:25.0	−268.5	200.5	Y	S6340C
J0650.4+2056	UGS	–	–	06:50:35.23	+20:55:56.8	−1715.0	−576.5	Y	S6340C
J0706.5+3744	GB6 J0706+3744	bzb	–	07:06:31.67	+37:44:36.7	−319.5	293.2	Y	S6340C
J0743.0+5446*	GB6 J0742+5444	bzq	0.72	07:42:46.10	+54:47:06.0	–	–	N	S6340C
J0745.2+7439	MS 0737.9+7441	bzb	0.32	07:44:05.45	+74:33:58.1	298.5	−155.0	Y	S6340E
J0745.2+8511	NVSS J074715+851208	agu	–	07:47:15.44	+85:12:08.2	−891.0	−422.0	Y	S6340E
J0828.9+0902	UGS	–	–	08:28:47.28	+09:03:37.3	–	–	N	S6340D
J0850.0+4849	GB6 J0850+4855	bzb	–	08:50:26.79	+48:52:00.7	873.1	−71.3	Y	S6340G
J0912.5+2758*	1RXS J091211.9+275955	bzb	–	09:12:20.81	+27:55:47.1	–	–	N	S6340D
J0930.4+8611	S5 0916+864	bzb	–	09:29:43.06	+86:12:21.3	−10.5	−18.5	Y	S6340E
J0946.2+0106*	RXS J094620.5+010459	bzb	0.56	09:46:19.81	+01:06:26.1	–	–	N	S6340G
J0959.5+6535	S4 0954+65	bzb	0.37	09:59:53.60	+65:34:57.0	−156.4	−518.1	Y	S6340G
J1023.6+2959*	RX J1023.6+3001	bzb	0.43	10:23:54.58	+29:58:00.4	–	–	N	S6340D
J1100.6+4018	RX J1100.3+4019	bzb	0.23	11:00:21.09	+40:19:27.7	274.5	−370.5	Y	S6340D
J1107.5+0223	BZB J1107+0222	bzb	–	11:07:35.99	+02:22:25.6	1112.5	1004.5	Y	S6340D
J1130.4+5814	BZB J1131+5809	bzb	0.36	11:31:18.69	+58:08:58.5	444.0	−302.0	Y	S6340D
J1135.7+6736*	RX J1136.5+6737	bzb	0.13	11:35:52.30	+67:37:24.2	–	–	N	S6340E
J1137.0+2553	RX J1136.8+2551	bzb	0.16	11:37:01.13	+25:51:33.8	−1320.5	−1603.5	Y	S6340G
J1212.2+2318	UGS	–	–	12:12:26.70	+23:14:18.9	487.9	−126.9	Y	S6340G
J1223.3+7953	UGS	–	–	12:23:58.22	+79:53:29.0	377.5	781.0	Y	S6340E
J1224.5+2437	MS 1221.8+2452	bzb	0.22	12:24:24.20	+24:36:23.6	134.0	60.5	Y	S6340E

Notes. Column 1: 1FHL name; Col. 2: low-frequency association of the 1FHL source; Col. 3: source classification: bzb = blazar of the BL Lac type, bzq = blazar of the FSRQ type, agu = active galaxy of uncertain type, snr = supernova remnant; Col. 4: redshift; Cols. 5 and 6: pointing coordinates; Cols. 7 and 8: RA and Dec. shift from the phase tracking center; Col. 9: detection; Col. 10: Experiment code. [(a)] Asterisks indicate the 8 sources excluded from the analysis because of incorrect pointing. [(b)] Coordinates of pointing.

Table A.1. continued.

IFHL name[a]	Assoc	Class	z	RA[b] h:m:s	Dec[b] d:m:s.	Shift RA mas	Shift Dec mas	Detection	Exp. code
J1244.9+5708	1RXS J124510.5+571020	bzb	–	12:45:09.99	+57:09:54.4	−0.5	−0.5	Y	S6340E
J1249.7+3706	RX J1249.8+3708	bzb	–	12:49:46.76	+37:07:48.0	140.0	88.0	Y	S6340E
J1310.9+0036	RX J1311.1+0035	bzb	–	13:11:06.42	+00:35:09.8	−841.0	−248.5	Y	S6340E
J1315.0+2346	TXS 1312+240	bzb	–	13:14:43.81	+23:48:26.8	–	0.5	Y	S6340D
J1322.9+2942*	4C +29.48	agu	–	13:23:02.59	+29:41:33.4	–	–	N	S6340D
J1406.4+1646	UGS	–	–	14:06:14.40	+16:46:35.0	–	–	N	S6340E
J1418.6+2539	BZB J1417+2543	bzb	0.24	14:17:56.27	+25:43:23.1	−5414.0	−3133.0	Y	S6340D
J1419.0+7730*	1RXS J141901.8+773229	agu	–	14:19:41.54	+77:34:43.6	–	–	N	S6340E
J1548.3+1455	UGS	–	–	15:48:24.34	+14:57:02.9	−669.5	184.5	Y	S6340D
J1619.8+7540	UGS	–	–	16:19:13.77	+75:37:53.8	100.0	347.5	Y	S6340E
J1631.0+5224	TXS 1629+524	bzb	–	16:30:43.12	+52:21:38.7	−261.5	105.5	Y	S6340D
J1735.9+2033	NVSS J173605+203301	bzb	–	17:35:41.48	+20:35:08.8	821.5	−193.0	Y	S6340H
J1744.2+1938	1ES 1741+196	bzb	0.08	17:44:15.87	+19:39:02.1	1797.8	−417.3	Y	S6340H
J1809.3+2040	RX J1809.3+2041	bzb	–	18:09:25.48	+20:41:31.0	394.0	101.1	Y	S6340F
J1841.1+2914	UGS	–	–	18:41:20.50	+29:11:28.5	130.2	−29.0	Y	S6340H
J1841.8+3219	RX J1841.7+3218	bzb	–	18:41:47.17	+32:18:38.6	1625.5	−555.0	Y	S6340F
J1911.0+0905	SNR G043.3-00.2	snr	–	19:11:03.97	+09:05:02.5	–	–	N	S6340H
J1926.9+6153	1RXS J192649.5+615445	bzb	–	19:26:49.95	+61:54:41.4	414.0	−946.5	Y	S6340F
J1942.8+1034	1RXS J194246.3+103339	agu	–	19:42:47.48	+10:33:27.8	−60.0	698.5	Y	S6340F
J2002.6+6303	UGS	–	–	20:02:44.96	+63:02:30.8	−2633.0	−2343.0	Y	S6340F
J2004.7+7003	UGS	–	–	20:04:41.67	+70:06:16.8	1464.7	1340.9	Y	S6340H
J2015.8+3710	VER J2016+372	bzq	0.86	20:15:53.68	+37:11:30.2	2.2	384.6	Y	S6340H
J2031.4+1941*	RX J2030.8+1935	agu	–	20:31:40.96	+19:40:34.0	–	–	N	S6340H
J2127.8+3614	B2 2125+35	bzb	–	21:27:43.04	+36:13:05.0	138.5	−736.0	Y	S6340F
J2212.5+2803	CRATES J221238+275944	agu	–	22:12:39.10	+27:59:38.5	0.5	4.5	Y	S6340F
J2223.4+0104	NVSS J222329+010226	bzb	–	22:23:29.59	+01:02:26.7	286.0	50.0	Y	S6340A
J2247.7+4412	NVSS J224753+441317	bzb	–	22:47:53.10	+44:13:17.0	−1133.0	1604.0	Y	S6340A
J2308.1+1459*	MG1 J230734+1449	bzb	0.50	23:07:59.07	+14:58:58.4	–	–	N	S6340H
J2314.0+1446	RGB J2313+147	bzb	0.16	23:13:57.27	+14:44:22.7	−918.5	−355.0	Y	S6340A
J2329.1+3754	NVSS J232914+375414	bzb	0.26	23:29:14.25	+37:54:14.9	−206.5	417.5	Y	S6340A
J2347.2+0707	CRATES J234639+07050	agu	–	23:47:06.48	+07:03:51.9	−1985.2	−2556.5	Y	S6340H

Table A.2. Details of the 67 detected sources.

IFHL name	RA	Dec	Class	S_γ	σ_{S_γ}	$S_{\rm NVSS}$	$\sigma_{S_{\rm NVSS}}$	$S_{\rm VLBI}$	$\sigma_{S_{\rm VLBI}}$	$T_{\rm B}$[a]
	h:m:s	d:m:s		10^{-12} erg/cm^2/s	10^{-12} erg/cm^2/s	mJy	mJy	mJy	mJy	10^9 K
J0007.7+4709	00:07:59.973	47:12:07.769	bzb	3.8	1.3	60.3	1.9	22.9	3.4	1.3
J0009.2+5032	00:09:22.760	50:30:28.847	bzb	12.3	3.8	11.8	0.5	5.8	0.9	0.5
J0037.8+1238	00:37:50.880	12:38:19.879	bzb	2.1	1.2	75.1	2.3	28.5	4.3	5.8
J0040.3+4049	00:40:13.978	40:50:07.145	bzb	8.8	5.6	47.3	1.8	1.5	0.2	>0.2
J0043.7+3425	00:43:48.843	34:26:26.093	bzq	7.6	3.3	92.8	2.8	106	16	80.5
J0053.9+4030	00:53:31.696	40:31:25.957	UGS	7.2	5.4	9.6	0.5	9.1	1.4	1.6
J0103.4+5336	01:03:25.958	53:37:13.279	agu	4.8	1.9	30.4	1.0	27.3	4.1	>32.3
J0131.3+6121	01:31:07.227	61:20:33.368	agu	19.5	5.4	19.1	0.7	6.2	0.9	>11.9
J0134.4+2643	01:34:28.196	26:38:43.025	agu	2.9	1.2	30.1	1.0	11.7	1.8	>16.9
J0153.1+7515	01:53:07.380	75:17:42.933	bzb	1.6	1.0	21.2	0.8	6.7	1.0	>7.8
J0213.1+2246	02:12:52.834	22:44:52.242	bzb	5.8	3.7	66.9	2.0	63.0	9.5	>61.6
J0241.3+6548	02:41:21.746	65:43:11.579	agu	4.9	2.3	190.3	5.7	24.0	3.6	1.6
J0307.4+4915	03:07:27.035	49:15:09.753	UGS	6.3	3.1	56.0	1.7	300	45	104
J0322.1+2337	03:21:59.970	23:36:11.206	bzb	9.1	4.6	76.2	2.3	28.5	4.3	>21.7
J0332.1+6307	03:31:53.916	63:08:14.160	UGS	3.2	1.8	42.2	1.3	18.9	2.8	2.4
J0333.6+2918	03:33:49.004	29:16:31.549	bzb	5.2	2.1	193.1	5.8	28.3	4.3	>4.6
J0334.0+6539	03:33:56.738	65:36:56.186	bzb	8.6	4.2	287.9	8.6	34.3	5.2	5.2
J0338.4+1304	03:38:29.279	13:02:15.449	UGS	10.6	5.9	15.1	0.6	6.13	0.94	>0.5
J0425.3+6320	04:25:25.356	63:20:01.681	UGS	3.9	2.5	24.1	1.2	0.44	0.08	>0.01
J0515.9+1528	05:15:47.353	15:27:16.592	bzb	6.7	3.6	26.5	0.9	31.6	4.8	>5.4
J0516.4+7351	05:16:31.232	73:51:08.659	bzb	4.8	3.4	55.5	1.7	8.5	1.3	>5.5
J0529.0+0937	05:29:02.614	09:34:31.180	agu	7.3	5.0	28.6	1.3	0.3	0.1	3.9
J0540.5+5822	05:40:30.009	58:23:38.452	bzb	6.5	3.5	29.3	1.0	11.7	1.8	>6.6
J0601.0+3838	06:01:02.869	38:38:29.170	UGS	7.3	5.1	704	21	62.4	9.4	92.9
J0605.0+0001	06:04:58.418	00:00:43.354	agu	2.5	1.0	34.4	1.1	8.8	1.3	0.5
J0605.4+2726	06:05:01.141	27:24:57.438	UGS	4.6	3.2	23.8	0.8	2.5	0.4	>0.2
J0644.2+6036	06:44:35.746	60:38:51.163	UGS	1.9	1.0	33.5	1.1	4.1	0.6	>0.4
J0648.9+1516	06:48:47.649	15:16:24.800	bzb	18.4	7.5	64.2	2.0	37.4	5.6	7.8
J0650.4+2056	06:50:35.352	20:55:57.376	UGS	4.5	2.9	6.4	0.5	4.6	0.7	>3.0
J0706.5+3744	07:06:31.697	37:44:36.407	bzb	10.4	4.3	27.0	0.9	14.7	2.2	>1.8
J0745.2+7439	07:44:05.375	74:33:58.255	bzb	3.4	1.9	22.6	0.8	16.3	2.4	>4.2
J0745.2+8511	07:47:16.148	85:12:08.614	agu	5.1	3.0	11.3	0.6	5.0	0.8	>0.8
J0850.0+4849	08:50:00.351	48:54:58.671	bzb	3.2	1.9	91.6	2.8	34.6	5.2	>1.0
J0930.4+8611	09:29:43.067	86:12:21.292	bzb	3.3	1.9	142.3	4.3	263	40	69.3
J0959.5+6535	09:58:47.245	65:33:54.818	bzb	3.1	2.1	729.4	21.9	402	60	26.6
J1100.6+4018	11:00:21.062	40:19:28.050	bzb	5.8	2.9	18.0	0.7	5.9	0.9	2.2
J1107.5+0223	11:07:35.916	02:22:24.595	bzb	2.4	1.3	20.8	0.8	7.9	1.3	>0.3
J1130.4+5814	11:31:18.629	58:08:58.792	bzb	1.5	1.0	42.6	1.3	21.2	3.2	>5.0
J1137.0+2553	11:36:50.128	25:50:52.403	bzb	7.2	4.8	14.7	0.6	3.3	0.5	0.1
J1212.2+2318	12:12:38.575	23:11:10.826	UGS	1.6	0.8	44.0	1.4	0.5	0.1	>0.01
J1223.3+7953	12:23:58.075	79:53:28.214	UGS	2.4	1.4	31.2	1.0	8.9	1.3	>9.4
J1224.5+2437	12:24:24.186	24:36:23.495	bzb	11.5	7.0	24.5	0.8	19.5	2.9	8.1
J1244.9+5708	12:45:09.999	57:09:54.373	bzb	1.2	0.7	83.3	2.5	66.9	10.0	5.5
J1249.7+3706	12:49:46.751	37:07:47.913	bzb	4.4	2.6	5.5	0.5	5.9	0.9	1.2
J1310.9+0036	13:11:06.476	00:35:10.046	bzb	3.9	2.2	17.2	0.7	15.7	2.4	3.6
J1315.0+2346	13:14:43.806	23:48:26.781	bzb	2.0	1.0	183.7	5.5	60.6	9.1	>52.8
J1418.6+2539	14:17:56.671	25:43:26.245	bzb	3.2	2.0	88.7	3.1	10.5	1.6	>1.8
J1548.3+1455	15:48:24.386	14:57:02.716	UGS	4.2	1.9	23.9	0.8	17.6	2.8	>1.0
J1619.8+7540	16:19:13.743	75:37:53.455	UGS	1.4	0.7	88.1	2.7	15.2	2.3	0.8
J1631.0+5224	16:30:43.146	52:21:38.624	bzb	3.1	2.0	120	4	18.9	2.9	>1.6
J1735.9+2033	17:36:05.261	20:33:01.192	bzb	5.9	3.4	24.3	0.8	5.8	0.9	0.3
J1744.2+1938	17:43:57.833	19:35:09.017	bzb	5.0	3.3	301.2	10.6	105.5	15.8	5.9

Notes. Column 1: source 1FHL name; Cols. 2 and 3: post-shift VLBI coordinates; Col. 4: source classification: bzb = blazar of the BL Lac type, bzq = blazar of the FSRQ type, agu = active galaxy of uncertain type, UGS = unassociated γ-ray source; Cols. 5 and 6: the 10−500 GeV energy flux of the γ-ray source and the relative 1-σ uncertainty; Cols. 7 and 8: 1.4 GHz NVSS flux density and the relative uncertainty; Cols. 9 and 10: 5 GHz VLBA peak flux density and the relative uncertainty (calculated by considering a calibration error of about 15% of the flux density and a statistical error provided by the map rms noise); Col. 10: brightness temperature. [(a)] For those sources whose radio core is unresolved, we calculate lower limits for the brightness temperature.

Table A.2. continued.

IFHL name	RA	Dec	Class	S_γ	σ_{S_γ}	$S_{\rm NVSS}$	$\sigma_{S_{\rm NVSS}}$	$S_{\rm VLBI}$	$\sigma_{S_{\rm VLBI}}$	$T_{\rm B}{}^a$
	h:m:s	d:m:s		10^{-12} erg/cm^2/s	10^{-12} erg/cm^2/s	mJy	mJy	mJy	mJy	10^9 K
J1809.3+2040	18:09:25.452	20:41:30.899	bzb	3.3	2.2	51.9	1.6	28.2	4.2	>4.2
J1841.1+2914	18:41:21.720	29:09:41.029	UGS	4.5	2.5	63.7	2.3	33.6	5.0	6.6
J1841.8+3219	18:41:47.042	32:18:39.154	bzb	4.6	2.1	20.4	0.7	10.4	1.6	>4.3
J1926.9+6153	19:26:49.891	61:54:42.344	bzb	10.5	2.9	22.1	0.8	18.5	2.8	6.8
J1942.8+1034	19:42:47.484	10:33:27.101	agu	20.7	8.1	98.6	3.0	48.6	7.3	8.6
J2002.6+6303	20:02:45.347	63:02:33.142	UGS	2.1	1.3	10.4	1.1	1.2	0.2	>0.01
J2004.7+7003	20:05:06.013	70:04:39.360	UGS	6.5	3.2	6.5	0.5	4.8	0.7	0.1
J2015.8+3710	20:15:28.730	37:10:59.515	bzq	8.3	3.8	2166	65	2501	250	145.5
J2127.8+3614	21:27:43.028	36:13:05.736	bzb	6.1	3.0	191.2	5.8	38.3	5.8	3.6
J2212.5+2803	22:12:39.103	27:59:38.441	agu	1.9	1.0	144.4	4.3	72	11	14.1
J2223.4+0104	22:23:29.571	01:02:26.650	bzb	1.5	1.1	6.1	0.5	6.3	1.0	1.5
J2247.7+4412	22:47:53.205	44:13:15.395	bzb	7.8	4.6	70.6	2.6	28.8	4.4	2.7
J2314.0+1446	23:13:57.333	14:44:23.055	bzb	8.8	5.0	40.6	1.3	14.8	2.3	0.7
J2329.1+3754	23:29:14.267	37:54:14.483	bzb	8.4	4.2	19.8	0.7	13.2	2.0	3.9
J2347.2+0707	23:46:39.933	07:05:06.856	agu	6.9	5.0	301.7	11.7	50.5	7.6	0.6